

BIT-DEPTH EXPANSION FOR NOISY CONTOUR REDUCTION IN NATURAL IMAGES

Akira Mizuno, Masayuki Ikebe

Graduate School of Information Science and Technology, Hokkaido University
Kita 14, Nishi 9, Kita-ku, Sapporo, 060-0814, Japan

ABSTRACT

We propose a bit-depth expansion (BDE) method targeting natural images. In the analog part of an imaging system, signal intensity fluctuations occur due to noise (e.g. thermal noise in the image sensor). After that, in the digital part, the intensities are rounded off to limited levels. The latter process, which is quantization, increases the intensity of fluctuation errors caused by stochastic resonance. These errors are viewed as false contour artifacts in the gradation region. Our goal was to obtain the original signal from the quantized noisy signal. We formulated a probabilistic model based on this quantization process, and successfully reconstructed smooth gradations from noisy contours. Subjective evaluation by voting clarified that the output image has higher quality.

Index Terms— Quantization, bit-depth expansion, false contours

1. INTRODUCTION

Bit-depth expansion (BDE) is desired in high dynamic range (HDR) imaging. Prior research on an HDR display system [1] has shown that more than 10 bits are necessary for the number of quantization levels to cover the desired range without quantization artifacts.

When displaying a relatively low bit-depth (LBD) image on a monitor, the brightness gets discontinuous values. Histogram equalization or other image enhancement methods may generate a sparse histogram. These discontinuities of brightness create an artifact called a false contour, appearing in low spatial frequency or low contrast regions such as the sky, sea, or skin. The false contour, which does not exist in the original scene, seriously degrades the image quality. Therefore, a method for reconstructing the original smooth gradation by interpolating the false contour is required. Coming up with an optimized reconstruction method is currently the most important issue in BDE.

Many attempts have been made to address this need in previous work. Low-pass filtering methods [2, 3, 4, 5, 6, 7, 8, 9] have been proposed to smooth the contour region. Dithering-based methods [7, 8, 10, 11] have been shown to reduce the visibility of undesirable artifacts. Flooding-based methods [12, 13, 14] can convert the 2D extrapolation problem into a 1D interpolation. Optimization-based methods [14, 15] maximize both accuracy and smoothness as much as possible. Some previous methods work well on images with no noise (e.g., computer graphics). Unfortunately, however, none of them can work on natural images.

Previous work's premise is that no noise is added to the original signal. In this case, the image quantization process is formulated as

$$\mathbf{y} = Q(\mathbf{x}), \quad (1)$$

where $\mathbf{x} = [x_1, x_2, \dots, x_n]^T \in \mathbb{R}^n$ is an original signal, $\mathbf{y} \in \mathbb{Z}^n$ is a quantized signal, and Q is a quantizer function defined as rounding

off fractions in this paper. Eq.(1) requires that the pixel values of an estimated signal is in per-pixel quantization bins:

$$x_i^* \in [y_i, y_i + 1), \quad (2)$$

where x_i^* is the estimated value of x_i ($1 \leq i \leq n$).

We use a more accurate formulation because natural images are inseparable from noise. The original signal is fluctuated by the noise before quantization:

$$\mathbf{y} = Q(\mathbf{x} + \xi), \quad (3)$$

where $\xi \in \mathbb{R}^n$ denotes the noise—it is stochastic variable generated from its distribution. Eq.(3) only states that the fluctuating signal is in the quantization bins:

$$x_i^* + \xi_i \in [y_i, y_i + 1). \quad (4)$$

Difference between the two quantization models Eq.(1) and Eq.(3) is constraint of the estimated signal \mathbf{x}^* . The constraint Eq.(2) from the model Eq.(1) restricts the value range of \mathbf{x}^* directly. On the other hand, Eq.(4) only requests the value range of $\mathbf{x}^* + \xi$. It does not decide the value range of estimated signal \mathbf{x}^* . This means that estimation out of range (i.e. $x_i^* \notin [y_i, y_i + 1)$) is allowed. The removing constraint of \mathbf{x}^* is an important point of this paper.

Figure 1 shows example results of BDE using the two different models, Eq.(1) and Eq.(3). The quantized signal (green) given from the fluctuating signal (cyan) is input for a BDE method. The quantized signal consists of some flat regions and noisy ones. A smooth sine-like curve is expected as a dequantized signal.

Then, the dequantized signals (blue or red) are obtained by two different methods. The methods for Figure 1(a) and Figure 1(b) are based on the models Eq.(1) and Eq.(3) respectively. Figure 1(a) is generated by one of flooding-based method [12], and Figure 1(b) by our method described later in this paper.

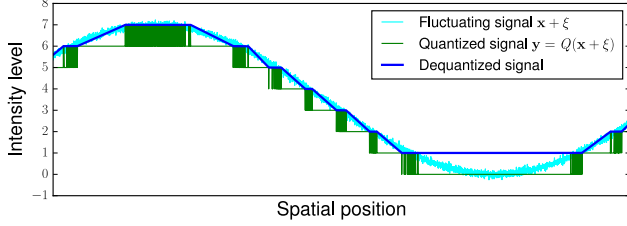
We can see that the result of Eq.(1) fails to reconstruct smooth gradations because the dequantized signal must be in quantization bins by reason of Eq.(2). The allowed range for dequantized signal, the quantization bins denoted as gray in Figure 1(c), is raised and collapsed incessantly at noisy area. Therefore, to achieve a continuous function, the dequantized signal is compelled to be flat by taking lower bounds of the raised bins and upper of the collapsed bins.

Because the result of Eq.(3) has smooth gradations, it is better. We explain the BDE method using Eq.(3) in this paper.

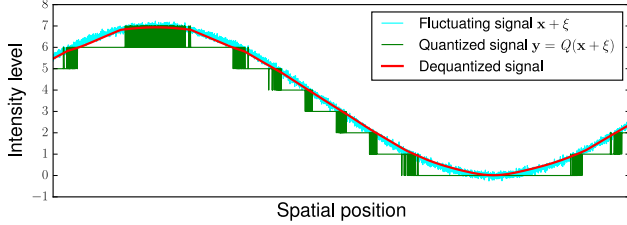
2. FORMULATION

Finding the most probable \mathbf{x} from an observed \mathbf{y} is an inverse problem of Eq.(3). We use the maximum a posteriori (MAP) estimation:

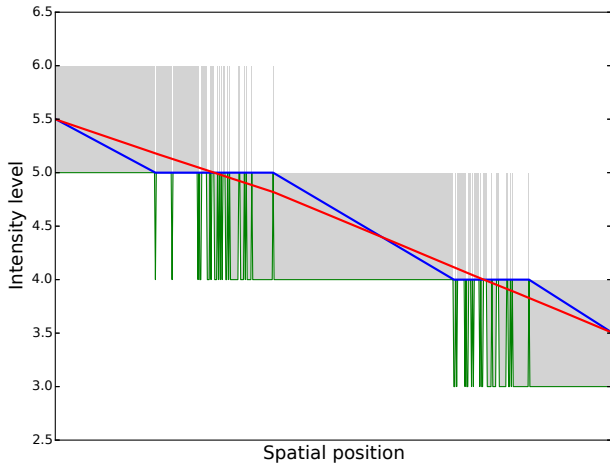
$$\mathbf{x}^* = \arg \max_{\mathbf{x}} Pr(\mathbf{y}|\mathbf{x})Pr(\mathbf{x}), \quad (5)$$



(a) Dequantization results by flooding-based method [12]



(b) Dequantization results by our method



(c) Zoom-in. The blue and red lines are the dequantization signals in (a) and (b) respectively. Please see that the blue line can not stray from quantization bins (gray).

Fig. 1. Example results of BDE methods based on different models Eq.(1) and Eq.(3)

where $Pr(\mathbf{y}|\mathbf{x})$ is a conditional probability of \mathbf{y} under the condition \mathbf{x} and $Pr(\mathbf{x})$ is a prior probability of \mathbf{x} .

One of the optimization-based methods [15] already applied the MAP estimation to dequantization, but the method still has the same kind of problem shown in Figure 1(a) because it uses the model Eq.(1). Our research solves the problem by using Eq.(3) instead of Eq.(1). In this section, we formulate the MAP estimation based on the model Eq.(3).

2.1. Prior probability

A prior probability $Pr(\mathbf{x})$ is formulated as a function to measure smoothness of \mathbf{x} .

First, we define an weight parameter $w_{i,j}$ between pixels y_i and

y_j in the quantized image \mathbf{y} as follows:

$$w_{i,j} = \begin{cases} 1 & (j \in \mathcal{N}_i \wedge |y_i - y_j| \leq \kappa), \\ 0 & \text{otherwise,} \end{cases} \quad (6)$$

where \mathcal{N}_i is a set of 4 nearest neighbors of the i -th pixel, and κ is a threshold parameter. In the image domain, $w_{i,j} = 1$ denotes that the pixels y_i and y_j are in the same region.

Using Eq.(6), we define a prior probability $Pr(\mathbf{x})$ as

$$W(\mathbf{x}) = \frac{1}{2} \sum_{i=1}^n \sum_{j=1}^n w_{i,j} (x_j - x_i)^2, \quad (7)$$

$$Pr(\mathbf{x}) = \exp\left(-\frac{W(\mathbf{x})}{2\sigma_s^2}\right), \quad (8)$$

where the function $W(\mathbf{x})$ means a total squared variation of the image \mathbf{x} segmented by $w_{i,j}$, and σ_s is a parameter to adjust the smoothness.

2.2. Likelihood

We formulate the likelihood using a distribution function of the noise ξ . The dominant noise from image sensor is known as shot noise. The shot noise follows a Poisson distribution. In this paper, we approximate the Poisson noise as a normal distribution. Thus, the probability distribution of $\tilde{x}_i = x_i + \xi_i$ is generated from x_i with added a stochastic variable ξ_i , $Pr(\tilde{x}_i|x_i)$, can be formulated as a common normal distribution function:

$$Pr(\tilde{x}_i|x_i) = \frac{1}{\sqrt{2\pi\sigma_g^2}} \exp\left(-\frac{(\tilde{x}_i - x_i)^2}{2\sigma_g^2}\right), \quad (9)$$

where σ_g is the variance of the distribution of ξ_i . From the definition of the quantization bin (Eq.(4)), y_i is generated when \tilde{x}_i is in range $[y_i, y_i + 1)$. Therefore the probability of y_i with given x_i , $Pr_l(y_i|x_i)$, can be calculated by accumulating $Pr(\tilde{x}_i|x_i)$ for all possible patterns of \tilde{x}_i as follows:

$$\begin{aligned} Pr_l(y_i|x_i) &= \int_{y_i}^{y_i+1} Pr(\tilde{x}_i|x_i) d\tilde{x}_i \\ &= \frac{1}{2} \left(\operatorname{erf}\left(\frac{y_i - x_i + 1}{\sqrt{2\sigma_g^2}}\right) - \operatorname{erf}\left(\frac{y_i - x_i}{\sqrt{2\sigma_g^2}}\right) \right), \end{aligned} \quad (10)$$

where $\operatorname{erf}(\cdot)$ is the error function. Figure 2 shows the function shapes of Eq.(10).

Here is another formulation for a special case. When y_i is a maximum (y_{\max}) or minimum (y_{\min}) value of its possible range, we can empirically estimate that the signal may be saturated. At the boundary of the signal range, we define the probability of y_i as

$$Pr_b(y_i|x_i) = \exp\left(-\frac{b_i(x_i)}{2\sigma_b^2}\right), \quad (11)$$

$$b_i(x_i) = \begin{cases} (y_{\min} - x_i)^2 & (y_i = y_{\min}), \\ (y_{\max} - x_i + 1)^2 & (y_i = y_{\max}), \\ 0 & \text{otherwise.} \end{cases} \quad (12)$$

The likelihood that $Pr(\mathbf{y}|\mathbf{x})$ is calculated by using Eq.(10) and Eq.(11) is as follows:

$$Pr(\mathbf{y}|\mathbf{x}) = \prod_{i=1}^n Pr_b(y_i|x_i) Pr_l(y_i|x_i). \quad (13)$$

The probability $Pr_b(y_i|x_i)$ works as a bias to shift the peak of probability $Pr_l(y_i|x_i)$.

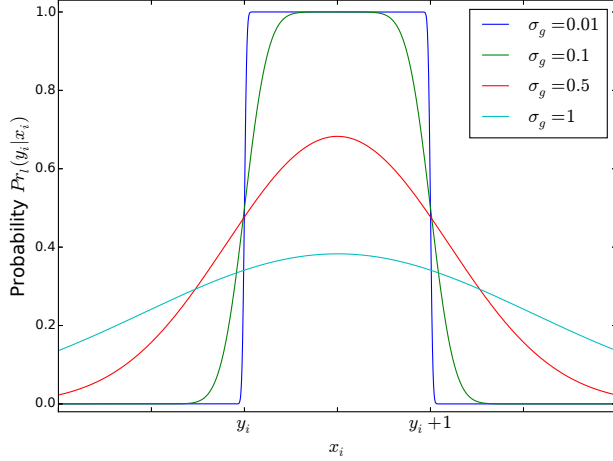


Fig. 2. Function shape of Eq.(10)

2.3. Optimization

We define the following optimization problem by combining Eq.(5), Eq.(8), and Eq.(13):

$$\mathcal{F} = \frac{1}{2\sigma_s^2} W(\mathbf{x}) + \frac{1}{2\sigma_b^2} \sum_{i=1}^n b_i(x_i) - \sum_{i=1}^n \log Pr_l(y_i|x_i), \quad (14)$$

$$\mathbf{x}^* = \arg \min_{\mathbf{x}} \mathcal{F}. \quad (15)$$

The partial derivatives of objective function \mathcal{F} are as follows:

$$\frac{\partial \mathcal{F}}{\partial x_i} = \frac{1}{2\sigma_s^2} W'_{x_i}(\mathbf{x}) + \frac{1}{2\sigma_b^2} b'_i(x_i) - \frac{Pr'_l(y_i|x_i)}{Pr_l(y_i|x_i)}, \quad (16)$$

$$W'_{x_i}(\mathbf{x}) = 2 \sum_{j=1}^n w_{i,j}(x_i - x_j), \quad (17)$$

$$b'_i(x_i) = \begin{cases} -2(y_{\min} - x_i) & (y_i = y_{\min}), \\ -2(y_{\max} - x_i + 1) & (y_i = y_{\max}), \\ 0 & \text{otherwise,} \end{cases} \quad (18)$$

$$Pr'_l(y_i|x_i) = \frac{1}{\sqrt{2\pi\sigma_g^2}} \left(-\exp\left(-\frac{(y_i - x_i + 1)^2}{2\sigma_g^2}\right) + \exp\left(-\frac{(y_i - x_i)^2}{2\sigma_g^2}\right) \right), \quad (19)$$

where $W'_{x_i}(\mathbf{x})$ is a partial derivative of the function $W(\mathbf{x})$ with respect to the variable x_i . The problem can be solved with the L-BFGS-B quasi-Newton method [16, 17, 18].

3. EXPERIMENTATION

We compared the results of the conventional methods and our method in Figure 4, Figure 5 and Table 1. The outputs were estimated from a quantized image. We evaluated their image qualities by calculating the peak signal to noise ratio (PSNR) and voting by

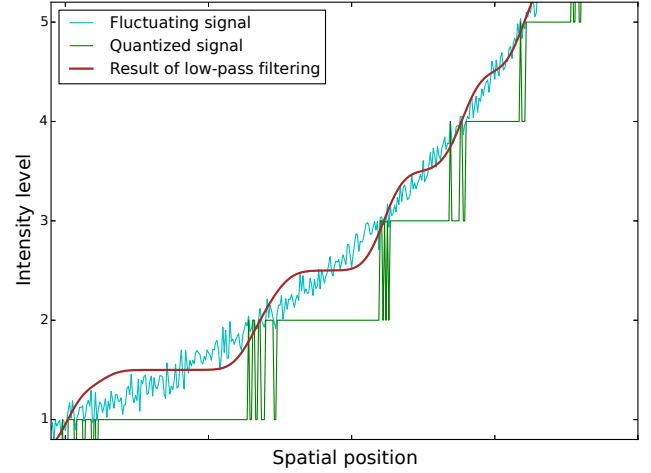


Fig. 3. Simulation of low-pass filtering

Table 1. Visual quality evaluation by voting

Image	Percentage of votes (%)		
	Wan 2012 [13]	Wan 2014 [15]	Proposed
Artificial I	12.9	6.5	80.6
Artificial II	22.6	16.1	61.3
Natural I	12.9	6.5	80.6
Natural II	6.5	3.2	90.3
Natural III	38.7	9.7	51.6

(Grayscale 4 → 8 bits, Number of samples = 31)

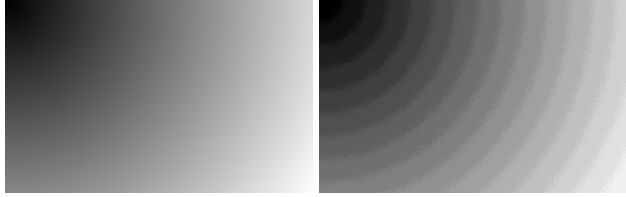
persons. Note that the PSNR values for Figure 5 can not be calculated because a ground-truth signal, namely a photograph without noise, can not be extracted from a natural image.

Two types of the conventional methods are compared with our method: the flooding-based one [13] and the optimization-based one [15]. The reason why the low-pass based methods are excluded is that they are not suitable to reconstruct smooth gradation from false contours. Figure 3 shows the simulation result of decontouring using a low-pass filter. When the flat region is in the input signal, the contour effect remains in the result. The low-pass filtering can remove high-frequency effects in quantized signal, but can not remove flat region because flat signal is completely low-frequency signal. The filter can only convert the step function (quantized signal in Figure 3) to the smoothed step function (result signal in Figure 3). Actually, we want to obtain a smooth slope-like function from a step function. Therefore, the low-pass based methods fails to reconstruct smooth gradation from large contours typically appearing in the sky, sea or skin.

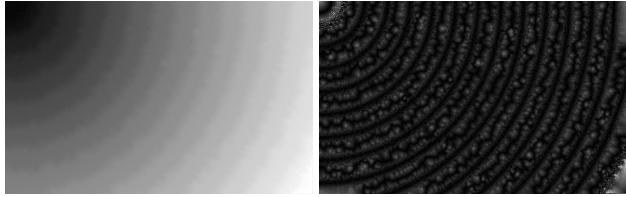
3.1. Experimental results

Figure 4 shows the results for artificial data. The original image was generated with additional noise in our computer. Then, the image was quantized and inputted into each method. The conventional methods can not reconstruct smooth gradation because of noise, but our method can.

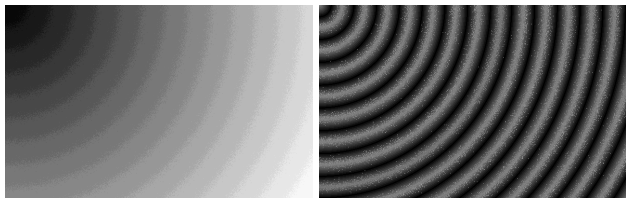
Figure 5 shows the results for a natural image. In the sky of the



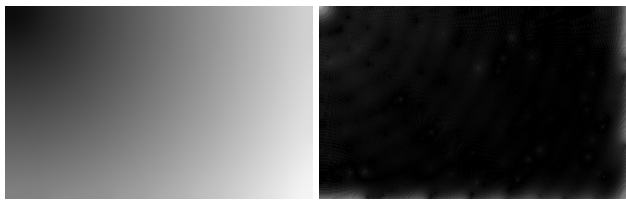
(a) Ground-truth (left) and quantized image after adding noises (right) of “Artificial I”



(b) Wan et al. (2012) [13] (PSNR:41.9 dB)



(c) Wan et al. (2014) [15] (PSNR:34.1 dB)



(d) Our method (PSNR:46.1 dB): $\kappa = 1$, $\sigma_s = 0.01$, $\sigma_g = 0.1$ and $\sigma_b = 0.5$

Fig. 4. Results and absolute error maps of BDE (grayscale 4 \rightarrow 8 bits) for an artificially generated data. For (b)–(d), the left column shows results and the right error maps against the ground–truth. The ranges of all error maps are amplified ($\times 16$) for visibility.

input image, false contour artifacts are evident. Our method sufficiently removed the artifacts (Figure 5(d)). This demonstrates that it can reconstruct smooth gradations efficiently.

Table 1 shows the visual quality evaluations by persons. The voters are presented three types of results which are outputs of Wan et al. (2012) [13], Wan et al. (2014) [15] and our method. And then, they choose one’s best image.

The voting was held on a specially prepared web site. Voters access to the site and look the images with their digital monitor. Two artificial images and three natural images were used for the voting. For artificial images, the ground-truth image is opened to voters, and they choose an image most similar to it. On the other hand, voting for natural images, original image is not opened. The voters can only see three output images, and they have to decide which one is a most quality photograph. The order of the output images are randomly shuffled for each voter. It is blind test because the voters are not able to know any identities about the images. As a result, most of the voters chose our method in every case.

Comparing their computational costs is not easy. They need to



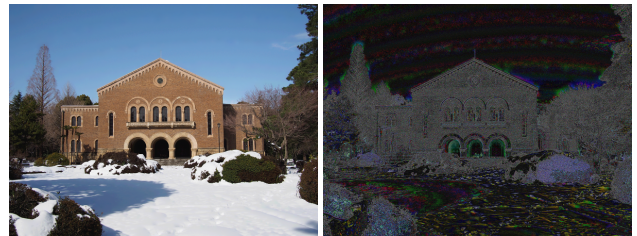
(a) Original (left) and quantized image (right) of “Natural I”



(b) Wan et al. (2012) [13]



(c) Wan et al. (2014) [15]



(d) Our method: $\kappa = 1$, $\sigma_s = 1$, $\sigma_g = 0.05$ and $\sigma_b = 1000$

Fig. 5. Results and absolute error maps of BDE (4 \rightarrow 8 bits / channel) for natural image. For (b)–(d), the left column shows results and the right error maps against the original.

use iterative algorithms for solving the problems. The number of iteration for Wan et al. (2012) [13] is depending on the width of false contour in input images. If input image has wide contour bands, large iteration number is required. Wan et al. (2014) [15] and our method are optimization-based approaches. The computational costs for them are depending on their parameters and input images.

4. CONCLUSION

We proposed a method for improving BDE quality for natural images. Our quantization model expresses the quantization process in natural image. We formulated an inverse quantization problem via MAP estimation focusing on noise distribution. Our method can recover smooth gradations from false contour artifacts.

5. REFERENCES

- [1] Helge Seetzen, Wolfgang Heidrich, Wolfgang Stuerzlinger, Greg Ward, Lorne Whitehead, Matthew Trentacoste, Abhijeet Ghosh, and Andrejs Vorozcovs, "High dynamic range display systems," in *ACM SIGGRAPH 2004 Papers*, New York, NY, USA, 2004, SIGGRAPH '04, pp. 760–768, ACM.
- [2] Akira Taguchi and Johji Nishiyama, "Bit-length expansion by inverse quantization process," in *Signal Processing Conference (EUSIPCO), 2012 Proceedings of the 20th European*, Aug. 2012, pp. 1543–1547.
- [3] Chun Hung Liu, O.C. Au, P.H.W. Wong, M.C. Kung, and Shen Chang Chao, "Bit-depth expansion by adaptive filter," in *IEEE International Symposium on Circuits and Systems, 2008. ISCAS 2008*, May 2008, pp. 496–499.
- [4] Scott J. Daly and Xiaofan Feng, "Decontouring: prevention and removal of false contour artifacts," in *Proc. SPIE, Human Vision and Electronic Imaging IX*, San Jose, CA, June 2004, vol. 5292, pp. 130–149, SPIE.
- [5] H.-R. Choi, J.W. Lee, R.-H. Park, and J.-S. Kim, "False contour reduction using directional dilation and edge-preserving filtering," *IEEE Transactions on Consumer Electronics*, vol. 52, no. 3, pp. 1099–1106, Aug. 2006.
- [6] Min-Ho Park, Ji Won Lee, Rae-Hong Park, and Jae-Seung Kim, "False contour reduction using neural networks and adaptive bi-directional smoothing," *IEEE Transactions on Consumer Electronics*, vol. 56, no. 2, pp. 870–878, May 2010.
- [7] Wonseok Ahn and Jae-Seung Kim, "Flat-region detection and false contour removal in the digital TV display," in *IEEE International Conference on Multimedia and Expo, 2005. ICME 2005*, July 2005, pp. 1338–1341.
- [8] Ning Xu and Yeong-Taeg Kim, "A simple and effective algorithm for false contour reduction in digital television," in *2010 Digest of Technical Papers International Conference on Consumer Electronics (ICCE)*, Jan. 2010, pp. 231–232.
- [9] Ji Won Lee, Bo Ra Lim, Rae-Hong Park, Jae-Seung Kim, and Wonseok Ahn, "Two-stage false contour detection using directional contrast and its application to adaptive false contour reduction," *IEEE Transactions on Consumer Electronics*, vol. 52, no. 1, pp. 179–188, Feb. 2006.
- [10] Cheuk-Hong Cheng, O.C. Au, Ngai-Man Cheung, Chun-Hung Liu, and Ka-Yue Yip, "Low color bit-depth image enhancement by contour-region dithering," in *IEEE Pacific Rim Conference on Communications, Computers and Signal Processing, 2009. PacRim 2009*, Aug. 2009, pp. 666–670.
- [11] S. Bhagavathy, J. Llach, and Jiefu Zhai, "Multiscale probabilistic dithering for suppressing contour artifacts in digital images," *IEEE Transactions on Image Processing*, vol. 18, no. 9, pp. 1936–1945, Sept. 2009.
- [12] Cheuk-Hong Cheng, O.C. Au, Chun-Hung Liu, and Ka-Yue Yip, "Bit-depth expansion by contour region reconstruction," in *IEEE International Symposium on Circuits and Systems, 2009. ISCAS 2009*, May 2009, pp. 944–947.
- [13] Pengfei Wan, Oscar C. Au, Ketan Tang, Yuanfang Guo, and Lu Fang, "From 2d extrapolation to 1d interpolation: Content adaptive image bit-depth expansion," in *2012 IEEE International Conference on Multimedia and Expo (ICME)*, July 2012, pp. 170–175.
- [14] Pengfei Wan, O.C. Au, Ketan Tang, and Yuanfang Guo, "Image de-quantization via spatially varying sparsity prior," in *2012 19th IEEE International Conference on Image Processing (ICIP)*, 2012, pp. 953–956.
- [15] Pengfei Wan, Gene Cheung, Dinei Florencio, Cha Zhang, and Oscar Au, "Image bit depth enhancement via maximum-a-posteriori estimation of graph AC component," Oct. 2014, IEEE Institute of Electrical and Electronics Engineers.
- [16] R. Byrd, P. Lu, J. Nocedal, and C. Zhu, "A limited memory algorithm for bound constrained optimization," *SIAM Journal on Scientific Computing*, vol. 16, no. 5, pp. 1190–1208, Sept. 1995.
- [17] Ciyu Zhu, Richard H. Byrd, Peihuang Lu, and Jorge Nocedal, "Algorithm 778: L-BFGS-b: Fortran subroutines for large-scale bound-constrained optimization," *ACM Trans. Math. Softw.*, vol. 23, no. 4, pp. 550–560, Dec. 1997.
- [18] Jos Luis Morales and Jorge Nocedal, "Remark on "algorithm 778: L-BFGS-b: Fortran subroutines for large-scale bound constrained optimization",," *ACM Trans. Math. Softw.*, vol. 38, no. 1, pp. 7:1–7:4, Dec. 2011.